

The Ca²⁺-binding protein sorcin stimulates transcriptional activity of the unfolded protein response mediator ATF6

Steven Z. Parks¹, Tian Gao^{1,*}, Natalia Jimenez Awuapura¹, Joseph Ayathamattam¹, Pauline L. Chabosseau¹, Dhananjaya V. Kalvakolanu², Héctor H. Valdivia³, Guy A. Rutter¹ and Isabelle Leclerc¹ 

1 Section of Cell Biology and Functional Genomics, Department of Metabolism, Digestion & Reproduction, Imperial College London, UK

2 Departments of Microbiology and Immunology, University of Maryland School of Medicine, Baltimore, MD, USA

3 Cardiovascular Research Center, University of Wisconsin-Madison, WI, USA

Correspondence

I. Leclerc, Section of Cell Biology and Functional Genomics, Department of Metabolism, Digestion & Reproduction, Imperial College London, London W12 0NN, UK

Tel: +44 (0) 207 594 3354

E-mail: i.leclerc@imperial.ac.uk

Present address

*Department of Molecular Mechanisms of Disease, University of Zurich, Switzerland

Steven Z. Parks and Tian Gao contributed equally to this work.

(Received 18 December 2020, revised 19 April 2021, accepted 21 April 2021, available online 24 May 2021)

doi:10.1002/1873-3468.14101

Edited by Hitoshi Nakatogawa

Sorcin is a calcium-binding protein involved in maintaining endoplasmic reticulum (ER) Ca²⁺ stores. We have previously shown that overexpressing sorcin under the rat insulin promoter was protective against high-fat diet-induced pancreatic beta-cell dysfunction *in vivo*. Activating transcription factor 6 (ATF6) is a key mediator of the unfolded protein response (UPR) that provides cellular protection during the progression of ER stress. Here, using nonexcitable HEK293 cells, we show that sorcin overexpression increased ATF6 signalling, whereas sorcin knock out caused a reduction in ATF6 transcriptional activity and increased ER stress. Altogether, our data suggest that sorcin downregulation during lipotoxic stress may prevent full ATF6 activation and a normal UPR during the progression of obesity and insulin resistance.

Keywords: ATF6; ER stress; lipotoxicity; sorcin

Obesity and its metabolic consequences are becoming a major threat to human health all over the world, causing life expectancy to fall for the first time in centuries [1]. Physical inactivity and nutrient oversupply increase circulating levels of glucose and free fatty acids, triggering endoplasmic reticulum (ER) stress through intensification of the cellular biosynthetic pathways in the pancreatic beta cell [2,3], but also in the liver [4], adipose tissue [5], skeletal muscle [6] and

hypothalamus [7]. ER stress is also implicated in the development of diabetes complications [8].

Sorcin (soluble resistance-related calcium-binding protein, gene name *SRI*, also known as CP-22, SCN and V19) is a member of the penta-EF-hand family of calcium-binding proteins that changes conformation in response to elevated calcium levels [9–15]. Sorcin was initially identified in multidrug-resistant cancer cells, is ubiquitously expressed and is highly conserved

Abbreviations

ap-FRET, acceptor-photobleaching FRET; ASGR1, asialoglycoprotein receptor 1; ATF6, activating transcription factor 6; BiP, binding immunoglobulin protein; CHOP, C/EBP homologue protein; CLuc, *Cypridina* luciferase; CO-IP, Co-immunoprecipitation; ER, endoplasmic reticulum; FRET, Förster/fluorescence resonance energy transfer; GRP78, glucose-regulated protein 78; HFD, high-fat diet; MEF, mouse embryonic fibroblast; RyR, ryanodine receptor; SERCA, sarco/endoplasmic reticulum Ca²⁺-ATPase; UPR, unfolded protein response; UPRE, unfolded protein response element.

amongst mammals [12,16]. In excitable cells such as cardiac myocytes and skeletal muscle cells, sorcin inhibits ryanodine receptor (RyR) activity [17] and plays a role in terminating Ca²⁺-induced Ca²⁺ release [18,19], an inherently self-sustaining mechanism which, if unchecked, may deplete intracellular Ca²⁺ stores [20]. Sorcin also activates sarco/endoplasmic reticulum Ca²⁺-ATPase (SERCA) pumps and ensures efficient refilling of ER Ca²⁺ stores after contraction [21].

We have recently reported that transgenic mice over-expressing sorcin in the pancreatic beta cell under the rat insulin promoter had improved glucose tolerance and beta-cell function when fed a high-fat diet (HFD) [22]. Beneficial effects of sorcin in the pancreatic beta cell included increased ER Ca²⁺ content, and glucose induced intracellular Ca²⁺ fluxes under lipotoxic conditions, but also an apparent increase in activating transcription factor 6 α (ATF6) signalling. ATF6 is a key mediator of the unfolded protein response (UPR) that provides cellular protection during the progression of ER stress [23–25]. Whether an active sorcin-ER Ca²⁺ component also exists in nonexcitable cells, where obesity-induced ER stress and depletion of ER Ca²⁺ stores are also observed [26,27], is not known at the moment.

Here, using the human cell line HEK293, we describe changes in endogenous sorcin expression during lipotoxic conditions and the effects of sorcin over-expression or inactivation on ATF6 signalling. Our data suggest that sorcin enhances the transcriptional activity of ATF6 and that sorcin downregulation during the progression of lipotoxicity might compromise ATF6 activity during ER stress.

Experimental procedures

Plasmids

Plasmid pSRIm containing murine sorcin cDNA under the control of CMV promoter has been described in Ref. [28]. Plasmid pSRImF112L was generated by site-directed mutagenesis (QuikChange kit, Agilent, Santa Clara, CA, USA) using the following primers: mSRI-F112L_F 5'CAA CAC TTC ATC AGT CTC GAT AGC GAT AGG AG and mSRI-F112F_R 5'CTC CTA TCG CTA TCG AGA CTG ATG AAG TGT TG. Plasmid pAdTrackSRI was described in Ref. [22]. Plasmid pAdTrackF112L was generated by site-directed mutagenesis using the following primers: hSRI-F112L_F 5'CAA CAC TTT ATC AGT CTT GAC ACT GAC AGG AG and hSRI-F112F_R 5'CTC CTG TCA GTG TCA AGA CTG ATA AAG TGT TG.

Plasmid p5xATF6-GL3 (Addgene #11976) is an unfolded protein response element (UPRE) *Firefly* luciferase reporter driven by five tandem repeats of ATF6-binding sites, plasmid p3xFLAG-ATF6 (Addgene #11975), contains the human ATF6 cDNA with an N-terminal 3xFLAG tag, plasmid pHA-GAL4-ATF6 contains an N-terminal HA epitope tag, the N-terminal 147 residues of yeast GAL4 fused to human ATF6 cDNA under the control of SV40 promoter and plasmid p5xGAL4-E1b-GL3 is a *Firefly* luciferase reporter driven by five GAL4 DNA-binding sites were kindly provided by Ron Prywes, Columbia University, and described in Ref.[29,30].

Plasmid pGluc/ATF6LD-CLuc is an expression vector encoding *Cypridina* luciferase (CLuc), a secreted luciferase, fused to the C-terminal luminal (intra-ER) domain of human ATF6 (amino acids 400–670), and plasmid pGluc/ASGR-CLuc is an expression vector encoding *Cypridina* luciferase fused to asialoglycoprotein receptor 1 (ASGR1), a slow maturing protein whose secretion is decreased in ER stress conditions, were kindly provided by Gökhan Hotamisligil, Harvard University, and described in Ref. [31]. They both also contain *Gaussia* luciferase (GLuc), another secreted luciferase, under a distinct CMV promoter, to normalize for transfection efficiency.

Plasmid pLV-CMV-XBP-Gluc, containing the first 558 nucleotides of human XBP1 coding sequence (containing the nonconventional XBP1 RNA splicing site by IRE1 α) fused to the last 504 nucleotides of GLucM43I, a detergent-resistant variant of the secreted *Gaussia* luciferase, was from Arnaud Zaldumbide, Leiden University and described in Ref. [32].

Plasmid YFP-SRI was generated by subcloning human sorcin cDNA taken from pAd-hSRI [22] into *KpnI*-*ApaI* sites of mVenusC1 (Addgene #27794). Plasmid ATF6-CFP, containing human ATF6 cDNA fused to mCerulean on the C-terminal side of ATF6, was generated by amplifying ATF6 ORF from pEGFP-ATF6 (Addgene #32955) by PCR using the following primers: Forward_5'-GTA CTC AGA TCT CGA GCT CAA GC and Reverse_5' TTT CCG GCC CGT TGT AAT GAC TCA GGG ATG GT (*ApaI* restriction site underlined). The resulting 2046-bp fragment was subsequently subcloned into mCeruleanN1 (Addgene #27795) using *HindIII* and *ApaI* restriction sites. YFP-SRI and ATF6-CFP constructs were verified by DNA sequencing.

Plasmid CFP-ATF6, containing human ATF6 cDNA fused to mCerulean on the N-terminal side of ATF6, was described in Ref. [33].

Plasmid C5V, a FRET reference standard containing a fusion protein between mCerulean and mVenus

separated by 5 amino acids, was from Steven Vogel (Addgene #26394) and described in Ref. [34]. pEGFP-C1 is an expression vector containing enhanced green fluorescent protein under the control of CMV promoter (Clontech®, Mountain View, CA, USA). pGL3-promoter is a transfection control containing firefly luciferase under the control of SV40 promoter from Promega® (Southampton, UK). pRL-CMV is a transfection normalization standard containing *Renilla* luciferase under the control of CMV promoter (Promega®). pG6PC2 and p3xNFAT are luciferase reporters described in Ref. [22]. Plasmid pSRI1, containing the proximal promoter of the human SRI gene (transcript variant 1, 198 aa) upstream of luciferase reporter gene, was generated by PCR using human genomic DNA and the following primers: Forward_5'-GAG TTC GGC CCT GAC ATC TA and Reverse_5'-GCA GTC GTC TCC AGC TCT TG. The resulting 1378-bp fragment was subcloned into pCR2.1 by TA cloning (Invitrogen, Carlsbad, CA, USA), digested by *KpnI*-*XhoI* and subcloned into pGL3basic (Promega) at the same restriction sites. DsRED2-ER-5 was a gift from Michael Davidson (Addgene #55836) and described in Ref. [35].

Cell culture and transfection

HEK293 cells (www.hek293.com) were maintained in Dulbecco's modified Eagle's medium (DMEM) containing 4.5 g·L⁻¹ glucose, 4 mmol·L⁻¹ L-glutamine, 100 IU·mL⁻¹ penicillin, 100 µg·mL⁻¹ streptomycin and 10% (vol/vol) FBS in a humidified atmosphere at 37 °C with 5% CO₂. HEK293 cells were transfected using the calcium phosphate coprecipitation method, pH 7.12.

Mouse embryonic fibroblasts (MEFs) were prepared from sorcin knockout (*Sri*^{-/-}) [22,36] and wild-type littermate embryos at E13.5-E15.5 day postcoitum essentially as described in Ref. [37] with the omission of DNase I in the digestion step and gelatine in the

plating step. Animals were kept at the Imperial College Central Biomedical Service and procedures approved by the UK Home Office Animals Scientific Procedures Act, 1986 (HO License PPL PA03F7F07). MEFs were cultured in DMEM containing 25 mM glucose, 4 mmol·L⁻¹ L-glutamine, 100 IU·mL⁻¹ penicillin, 100 µg·mL⁻¹ streptomycin and 10% (vol/vol) FCS in a humidified atmosphere at 37 °C with 5% CO₂. MEFs were transfected with Xfect® (Clontech) as per manufacturer's instructions. Experiments were performed on MEFs between passages 4 and 20.

CRISPR/Cas9 gene editing

For generating *SRI*-null HEK293 cells, oligonucleotides encompassing guide RNA sequences from the human *SRI* gene located in exon 3 at position 37 (hSRI_Ex3_37Sens: 5'CAC CGC TGA CAC AGT CTG GCA TTG C, hSRI_Ex3_37ASens: 5'AAA CGC AAT GCC AGA CTG TGT CAG) were annealed and phosphorylated before subcloning in pX330 at *BsbI* as described in Ref. [38]. The resulting pX330-hSRI-Ex3-37 plasmid was verified by sequencing before transfection in HEK cells. Twenty-four hours after transfection, the cells were seeded into 96-well plates at a density of ≤1 cell/well for clonal selection. *SRI* gene disruption was confirmed by qRT-PCR and western blotting on selected clones.

RNA extraction and qRT-PCR

Total RNA extraction and qRT-PCR were performed as in Ref. [39] using the primers listed in Table 1.

Western blots

Protein extraction was performed in ice-cold RIPA buffer containing 50 mM Tris/HCl pH 7.4, 150 mM NaCl, 1% NP-40, 0.1% SDS, 0.5% Na deoxycholate and Roche® (Basel, Switzerland) Complete Proteases

Table 1. List of qPCR primers

Gene name	Forward qPCR primer (5'→3')	Reverse qPCR primer (5'→3')
ATF6	GCTGCAATTGGAAGCAGCAA	TGTCCCAAATGTCTGACTCCC
β-actin	TCCCTGGAGAAGAGCTACGA	AGCACTGTGTTGGCGTACAG
CHOP	ACCAAGGGGAGAACCCAGGAAACG	TCACCATTCCGGTCAATCAGAGC
EDEM1	TTCCCTCCTGGTGAATTT	AGGCCACTCTGCTTTCCAAC
GAPDH	GGGAAGGTGAAGGTCGGAGT	TTGAGGTCAAGAAGGGGTCA
GRP78/BiP	GCCTGTATTTCTAGACCTGCC	TTCATCTTGCCAGCCAGTTG
HERPUD1	AACGGCATGTTTTGCATCTG	GGGGAAGAAAGGTTCCGAAG
SEL1L	ATCTCAAAGGCAGCAAGC	TGGGAGAGCCTTCCTCAGTC
SRI	AGATGCTGATGAATTGCAGAG	TCATTGAAACCCATTGTGCC
WFS1	GTTCCCGACTCAATGCCACA	CCGTGCGTCTCTAACACC

Table 2. List of antibodies used

Antigen	Host species	Source	Dilution used
ATF6	rabbit	Abcam 122897	1 : 500
Flag	mouse	Sigma F1804	1 : 1000
GAPDH	rabbit	Cell Signaling 14C10	1 : 50 000
GFP	mouse	Sigma G6795	1 : 1000
GRP78/BiP	rabbit	Abcam 21685	1 : 1000
Sorcin	rabbit	In-house ref [19]	1 : 15 000
Tubulin	mouse	Sigma T5168	1 : 10 000

Inhibitors. Cells were left to lyse on ice for 30 min before sonication for 10 s and centrifuged at 16 000 *g* for 20 min at 4 °C. Protein concentration assay was performed using Pierce® (Loughborough, UK) BCA kit. Ten to 25 µg of protein was loaded on 10% acrylamide mini gels, transferred on PVDF membranes and incubated with specific antibodies listed in Table 2. Quantification of bands intensity was performed using IMAGEJ software (<https://imagej.nih.gov/ij/download.html>).

Co-immunoprecipitation

HEK293 cells were transfected with either CFP-ATF6 or ATF6-CFP or empty vectors for 48 h before cell lysis and immunoprecipitation using Alpaca GFP-Trap® (ChromoTek, Planegg-Martinsried, Germany) according to manufacturer's instructions. Immunoblotting was performed using our antisorcin antibody or anti-glucose-regulated protein 78 (GRP78)/binding immunoglobulin protein (BiP; Abcam ab 21685, Cambridge, MA, USA, 1 : 1000), a known interactor of ATF6, as positive control.

Cytosolic calcium imaging

Imaging of free cytosolic Ca²⁺ concentration ([Ca²⁺]_{cyt}) in HEK293 WT and *SRI*-null cells was performed using the trappable intracellular fluorescent Ca²⁺ dye Fura-2-AM (Invitrogen) as described in Ref.[40]. Briefly, cells were perfused for 4 min at a constant 37 °C with Krebs-Ringer bicarbonate HEPES buffer (KRBH, 125 mmol·L⁻¹ NaCl, 3.5 mmol·L⁻¹ KCl, 1.5 mmol·L⁻¹ CaCl₂, 0.5 mmol·L⁻¹ MgSO₄, 0.5 mmol·L⁻¹ NaH₂PO₄, 2.0 mmol·L⁻¹ NaHCO₃, 10 mmol·L⁻¹ HEPES) supplemented with 25 mmol·L⁻¹ glucose/0.1% (wt/vol) BSA, before buffer change to KRBH buffer containing 0.1 µM thapsigargin (Sigma-Aldrich, Gillingham, UK, 586005). Imaging data were analysed with IMAGEJ software using an in-house macro (available on demand), and the fluorescence emission ratios were derived after subtracting background fluorescence.

Luciferase reporter assays

Firefly and *Renilla* luciferases were assayed from whole cell lysates with the Dual-Luciferase® Reporter Assay System (Promega) as per manufacturer's instructions. *Cypridina* luciferase was assayed from undiluted cell culture supernatants using Pierce® Cypridina Luciferase Glow Assay Kit (Thermo Scientific, Loughborough, UK) or BioLux® Cypridina Luciferase Assay Kit (New England Biolabs, Ipswich, MA, USA), and *Gussia* luciferase was assayed from 1 : 40 diluted cell culture supernatant using either the Stop & Glo reagent from the Dual-Luciferase® Reporter Assay System (Promega) or BioLux® Gussia Luciferase Assay Kit (New England Biolabs) in a Lumat LB 9507 luminometer (Berthold Technologies, Bad Wildbad, Germany).

FRET and confocal imaging studies

For the ap-FRET studies, wild-type HEK293 cells were plated coverslips and transfected overnight with equal amount of mCerulean and mVenus constructs as indicated before medium change containing ± 0.03 µM thapsigargin to activate ATF6 for a further 24 h. Some cells were treated with 1 µM ionomycin to increase intracellular Ca²⁺ for 1 h prior to fixation by incubation with 4% PFA for 20 min, washing in PBS and distilled water and mounting on slides using ProLong Diamond Antifade Mountant (Invitrogen). Acceptor-photobleaching FRET (ap-FRET) was performed on an LSM 780, AxioObserver confocal microscope, and images were acquired using a 63×/1.40 Oil DIC Plan-Apochromat objective. Highlighted regions of interest (ROIs) of ~ 7 µm were drawn over cells expressing both constructs. Fluorophores were stimulated with a 405 nm laser and emission split using a CFP and YFP filter. Five images were acquired before and 10 images after photobleaching to confirm stable fluorescence intensity of mCerulean. Highlighted ROIs were photobleached using a 514 nm laser line at 100% intensity for 20 iterations to destroy mVenus acceptor. Images were processed using IMAGEJ, and FRET efficiency was calculated using the formula below.

$$\text{FRET Efficiency (\%)} = 100 \times \frac{\text{mCerulean Emission Post PB} - \text{mCerulean Emission Pre PB}}{\text{mCerulean Emission Post PB}}$$

For the confocal colocalization studies, wild-type HEK293 cells on coverslips were transfected with both YFP-SRI and DsRed2-ER-5, an ER marker. Cells were fixed with DAPI and imaged as above using ZEN IMAGING software. Fluorophores were stimulated using

405 nm, 488 nm and 543 nm lasers, and images were acquired and processed using IMAGEJ.

Crude subcellular fractionation

Fractions enriched for cytosolic and membrane bound organellar proteins were obtained by sequential lysis in digitonin-containing buffer followed by lysis of the remaining pellet in NP40-containing buffer to solubilize intracellular membrane bound organelles such as the ER, essentially as described in Ref.[41]. Extracted proteins from each fraction were analysed by western blot using our anti-sorcin antibody. An anti-GAPDH antibody (Cell Signaling 14C10, Danvers, MA, USA) was used as a marker of the cytosol and an anti-GRP78/BiP antibody (Abcam ab21685) as a marker of the ER. The location of exogenously expressed mVenus-Sorcin and mCerulean-ATF6 was determined using an anti-GFP antibody (Sigma G6795).

Statistical analysis

All results are presented as means \pm SEM of at least 3 independent experiments. Differences between means

were analysed by two-tailed unpaired Student's *t*-test or two-way ANOVA as specified. *, ** and *** indicate $P < 0.05$, 0.005 and 0.001 , respectively.

Results

Palmitate reduces sorcin expression, and sorcin ablation causes ER stress in HEK293 cells

Having previously documented that sorcin protects against lipotoxicity-induced ER Ca^{2+} depletion in pancreatic beta cells [22], we next sought to investigate whether such mechanism would also take place in nonexcitable cells. As anticipated, prolonged incubation (72 h) of HEK293 cells with palmitate resulted in a decrease in sorcin mRNA levels (Fig. 1A, mRNA sorcin fold change, 72 h palmitate vs control, 0.70 ± 0.06 , $P < 0.005$, $n = 5$) and protein levels (Fig. 1B,C, protein sorcin fold change, 72 h of palmitate vs control, 0.84 ± 0.002 , $P < 0.005$, $n = 7$).

We then removed sorcin in the human cell line HEK293 by CRISPR/Cas9-mediated genome editing to generate *SRI*-null HEK293 cells to readily explore the biological effects of sorcin (Fig. 1D).

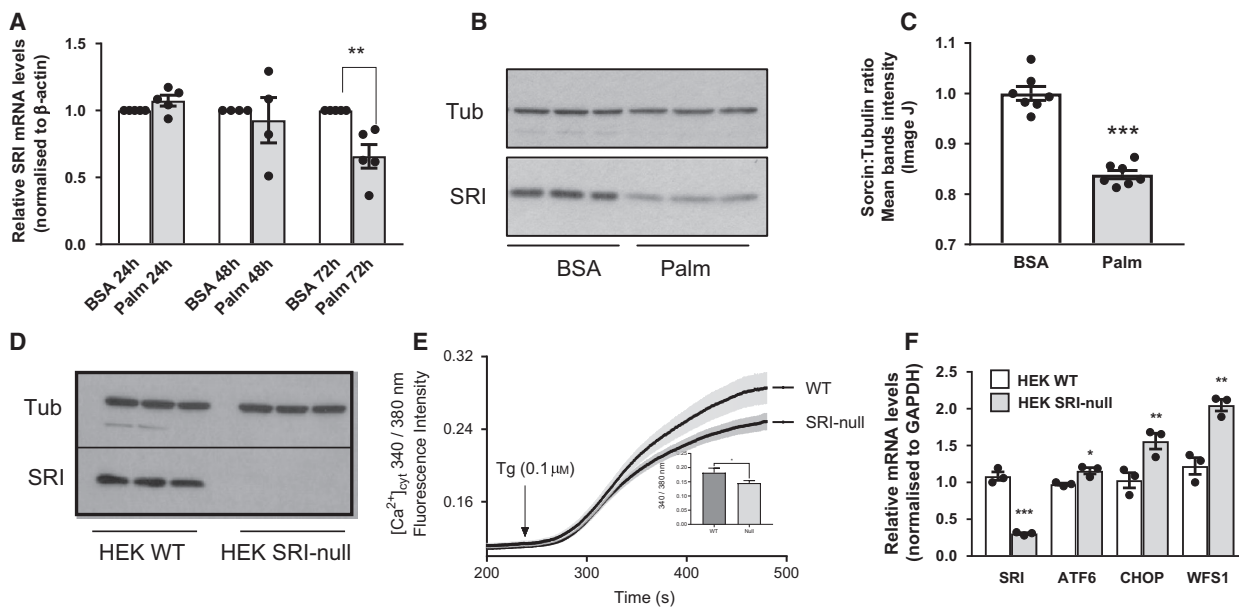


Fig. 1. Palmitate reduces sorcin expression, and sorcin ablation causes ER stress in HEK293 cells. (A) qRT-PCR analysis of sorcin expression in HEK293 cells incubated in the presence of $500 \mu\text{M}$ palmitate or BSA vehicle for 24 h, 48 h and 72 h as indicated. (B) Representative western blot and (C) quantification of three independent western blots of HEK293 cells incubated in the presence of $500 \mu\text{M}$ palmitate for 72 h before immunoblotting using antitubulin and antisorcine antibodies as indicated. (D) Representative western blot of sorcin and tubulin immunoreactivity in WT and *SRI*-null HEK293 cells. (E) Traces of cytosolic Ca^{2+} concentration measured by the ratio of fluorescence emission upon excitation at 340/380 nm as described in Methods. The inset graph shows the net increase in fluorescence emission before and after thapsigargin administration in WT and *SRI*-null cells (WT vs null, $n = 58$ vs 80 cells, $P < 0.05$). (F) qRT-PCR analysis of mRNA levels of SRI, ATF6, CHOP and WFS1 in WT and *SRI*-null HEK293 cells. Results are expressed as means \pm SEM of ≥ 3 independent experiments; * $P < 0.05$, ** $P < 0.005$ and *** $P < 0.001$ by two-tailed unpaired Student's *t*-tests.

HEK293 cells appeared normal in shape but were growing roughly 10%–15% more slowly than their WT counterparts transfected with an empty plasmid and hereafter used as control cells (not shown).

Mirroring the known role of sorcin in excitable cells, sorcin ablation in HEK293 cells reduced thapsigargin-induced elevation in cytosolic Ca^{2+} , indicating a lower ER Ca^{2+} content, compared to WT cells (Fig. 1E). *SRI*-null HEK293 cells also exhibit a low-grade basal ER stress as measured by the increase expression of some ER stress markers, namely ATF6, C/EBP homologue protein (CHOP) and Wolfram (WSF1; Fig. 1F).

Sorcin enhances ATF6 signalling independently of effects on Ca^{2+} dynamics

We next examined ATF6 signalling in response to modification of sorcin expression levels. ATF6 is a large 90 kDa protein anchored at the ER membrane, which translocates to the Golgi apparatus in response to ER stress. Once in the Golgi, it is cleaved to release a smaller 50 kDa active protein, which enters the nucleus and acts as a transcription factor [30]. Therefore, to assay ATF6 activation, we used two different ATF6 reporter luciferase plasmids, namely p5xATF6-GL3 [29], which contains five tandem repeats of ATF6-binding site and can be activated by endogenous or overexpressed ATF6 (Fig S1A), and p5xGAL4-Elb-GL3 [30], a GAL4 reporter gene which is exclusively activated by cotransfection with a GAL4 fusion protein, here GAL4-ATF6. The latter was used in order to circumvent any possible nonspecific binding on p5xATF6-GL3 reporter by other transcription factors such as XBP1s [42], and to specifically measure ATF6 activity in response to sorcin changes.

As shown in Fig. 2, cotransfection with sorcin increased the activity of the UPRE reporter p5xATF6-GL3 1.8-fold ($P < 0.001$, $n = 6$; Fig. 2A) and of p5xGAL4-Elb-GL3 7.2-fold ($P < 0.001$, $n = 4$ –5; Fig. 2B) compared with cotransfection with GFP, used as an inert control protein. Conversely, in *SRI*-null HEK293 cells, the activity of both p5xATF6-GL3 and p5xGAL4-Elb-GL3 reporters was reduced by 28% and 26%, respectively, compared to WT HEK293 cells ($P < 0.001$, $n \geq 3$; Fig. 2C,D). A similar result was obtained in MEF cells prepared from sorcin knockout (KO) embryos, where the activity of p5xATF6-GL3 reporter was decreased by 57% ($P < 0.001$, $n = 5$) in basal conditions and by 61% ($P < 0.05$, $n = 5$) in cells stimulated by thapsigargin, compared to WT MEFs (Fig. 2E). The absence of sorcin did not affect the luciferase synthesis driven by four unrelated promoters,

namely pGL3basic, pG6PC2, pSRI1 and p3xNFAT reporter (Fig. S1B).

In order to exclude a subsidiary Ca^{2+} storage effect of sorcin on ATF6 activation, we used the naturally occurring sorcin mutant F112L that disrupts one of the two high-affinity E-F hand Ca^{2+} -binding domains, resulting in a sixfold decrease in calcium affinity, impairment of protein–protein interactions [43], and also impaired capacity of the variant to translocate to the membrane fraction, at least *in vitro* [44]. As shown in Fig. 2F, both sorcin WT and F112L stimulated the UPRE reporter p5xATF6-GL3 to the same degree, either in HEK WT cells or in HEK *SRI*-null cells despite exhibiting different calcium kinetics in response to thapsigargin in HEK *SRI*-null cells (Fig. 2G). Indeed, re-expressing the F112L mutant for 48 h resulted in a quicker (Fig. 2G,J) and higher (Fig. 2G, H) release of Ca^{2+} from the ER following thapsigargin treatment compared with WT sorcin, without changing basal cytosolic Ca^{2+} (Fig. 2G,I). The latter results would argue against a Ca^{2+} effect of sorcin on ATF6 activation.

Sorcin ablation reduces ATF6 activity despite increasing ER stress

We next used a combination of plasmids to measure both specific ATF6 activation and overall cellular ER stress, independently, as described by Fu *et al.* [31]. pGLuc/ATF6LD-CLuc encodes *Cypridina* luciferase (CLuc), a secreted luciferase, fused to the C-terminal luminal (intra-ER) domain of ATF6, and pGLuc/ASGR-CLuc encodes *Cypridina* luciferase fused to ASGR1, a slow maturing protein whose secretion is decreased in ER stress conditions [45]. Both plasmids also contain *Gaussia* luciferase (GLuc), another secreted luciferase, under a distinct CMV promoter, to normalize for transfection efficiency. Typically, secretion of both ATF6LD-CLuc and ASGR-CLuc is inversely correlated, as ATF6LD-CLuc secretion increases under conditions of ER stress, whereas ASGR-CLuc secretion decreases [31]. We hypothesized that, in the absence of sorcin, both proteins would be less secreted, as this should increase ER stress but also dampen ATF6 activation. Indeed, as shown in Fig. 3 A,B, the secretion of ATF6LD-CLuc and ASGR-CLuc increased and decreased, respectively, following the induction of ER stress with thapsigargin in both WT and *SRI*-null HEK293 cells as expected. However, at low doses thapsigargin, the secretion of ATF6LD-CLuc and ASGR-CLuc was both reduced in *SRI*-null HEK293 cells compared with WT HEK cells, by 45% and 52%, respectively; however, the difference between

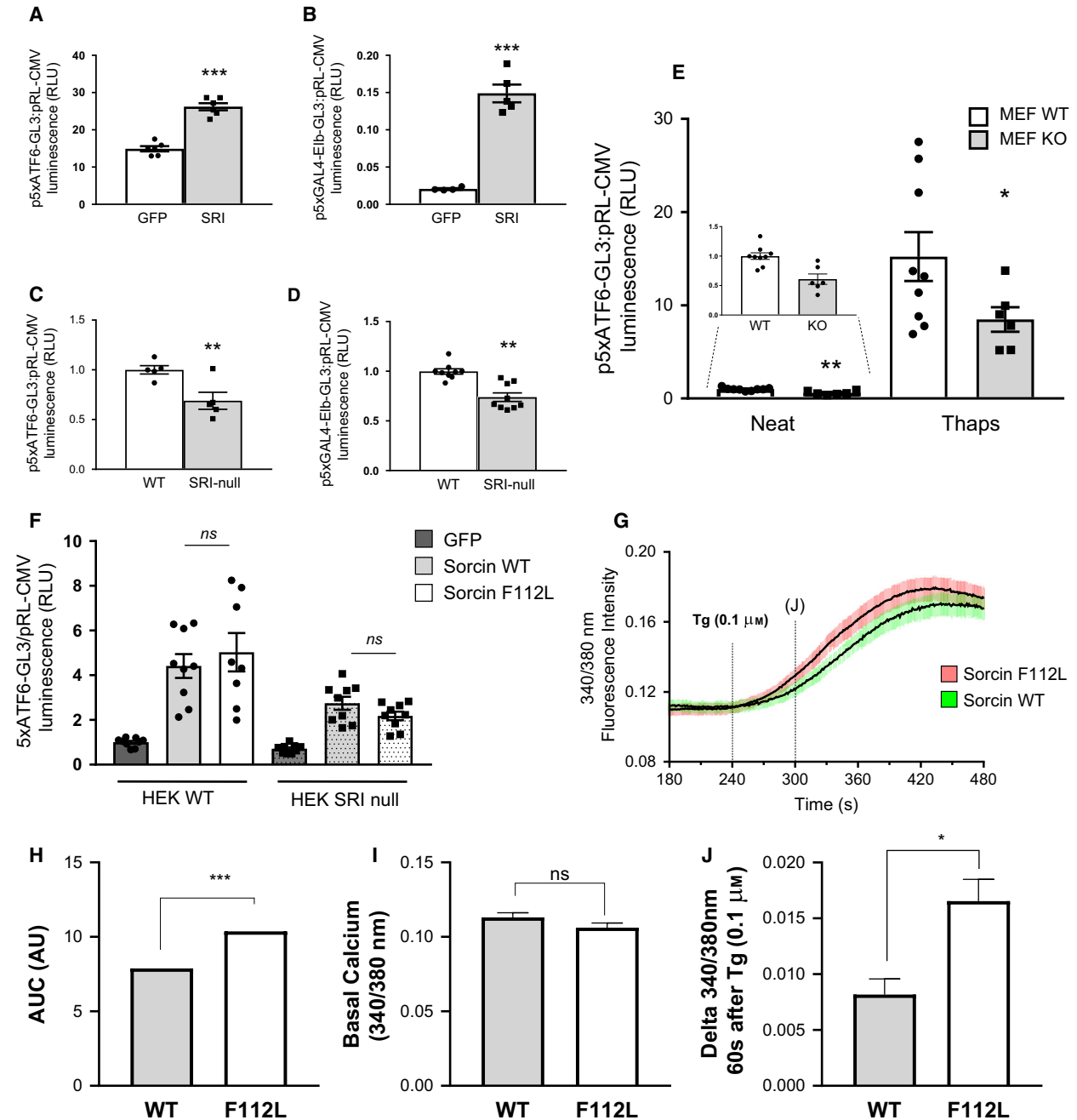


Fig. 2. Sorcin stimulates ATF6 activity (A, B) HEK293 cells were cotransfected with p5xATF6-GL3 reporter plasmid (A) or with p5xGAL4-EIb-GL3 and pHA-GAL4-ATF6 (B) and either GFP or SRI expression vector as indicated for 48 h before cell lysis and luciferase assays. (C, D) WT and *SRI*-null HEK293 cells were transfected with p5xATF6-GL3 (C) or p5xGAL4-EIb-GL3 and pHA-GAL4-ATF6 (D) for 48 h before cell lysis and luciferase assays. (E) SRI WT and KO MEFs were transfected with p5xATF6-GL3 as in (C) for 24 h before medium change containing \pm thapsigargin $0.1 \mu\text{M}$ as indicated for a further 24 h before cell lysis and luciferase assay. (F) WT and *SRI*-null HEK293 cells were cotransfected with p5xATF6-GL3 and either GFP or Sorcin WT or F112L mutant expression vector as indicated for 48 h before cell lysis and luciferase assays. (G) Traces of cytosolic Ca^{2+} concentration measurements in *SRI*-null HEK293 cells transfected with either pAdTrackSRI or pAdTrackF112L for 48 h as described in methods. (H) Area under the curve (AUC) of net calcium increased calculated for both constructs, using the average 340/380 ratio from 0 to 240 s as the baseline value. (I) Basal cytosolic Ca^{2+} calculated by average 340/380 ratio before thapsigargin administration (0–240 s). (J) Rate of calcium loss from the ER calculated by measuring the delta increase from basal cytosolic Ca^{2+} (340/380) 60 s after thapsigargin administration. Results are expressed as means \pm SEM of ≥ 3 independent experiments, imaging between 19 and 25 cells per condition (G–J), repeats were then selected based on GFP intensity (2000–6000 AU) and response to thapsigargin (Sorcin WT vs Sorcin F112L, $n = 47$ vs 31). Significance was calculated using Tukey's multiple comparison test and ANOVA, * $P < 0.05$, *** $P < 0.001$.

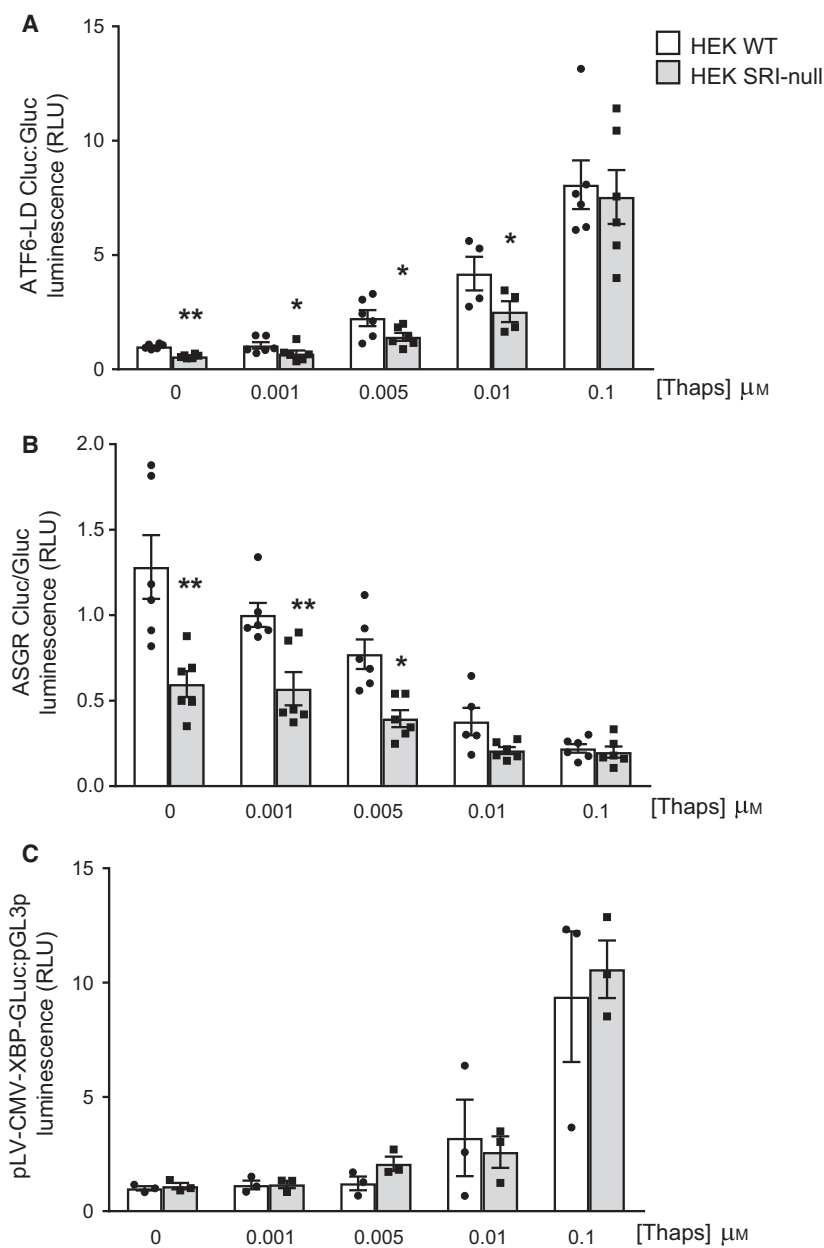


Fig. 3. Sorcin ablation decreases ATF6 activation despite increasing ER stress. (A–C) WT and *SRI*-null HEK293 cells were transfected with pGluc/ATF6LD-CLuc (A) pGluc/ASGR-CLuc (B) or pLV-CMV-XBP-GLuc and pGL3p (C) for 24 h before medium change containing increasing doses of thapsigargin as indicated for a further 24 h before luciferase assays as described in Methods. Results are expressed as means \pm SEM of ≥ 3 independent experiments, * $P < 0.05$, ** $P < 0.005$ by two-tailed unpaired Student's *t*-tests.

the genotypes was lost at higher dose of thapsigargin (0.1 μM). In order to exclude a nonspecific effect of overall diminished secretion of luciferase in sorcin-null cells, possibly through sluggish ER capacity, we next used a similar luciferase fusion plasmid, namely pLV-CMV-XBP-GLuc, which encodes an XBP-1 splicing reporter [32]. Upon ER stress, the splicing of XBP-1 RNA by IRE1 α positions the *Gaussia* luciferase coding sequence in frame with the XBP1 *bona-fide* AUG to generate XBP-*Gaussia* luciferase fusion protein. As shown in Fig. 3C, thapsigargin stimulated the secretion of XBP-*Gaussia* similarly in both *SRI*-null HEK293

and WT HEK293 cells, excluding a nonspecific effect of sorcin on protein secretion and confirming our previous results in MIN6 cells showing no effect of sorcin on XBP-1 splicing [22].

Having shown that sorcin was necessary for full ATF6 activity using luciferase reporters, we next measured expression of endogenous ATF6 target genes in *SRI*-null HEK293 cells in response to ER stress. As shown in Fig. 4, the induction of ATF6 target genes GRP78, SEL1L, EDEM1 and HERPUD1 was reduced in *SRI*-null cells in response to thapsigargin (Fig. 4C–F). On the contrary, sorcin's absence did not

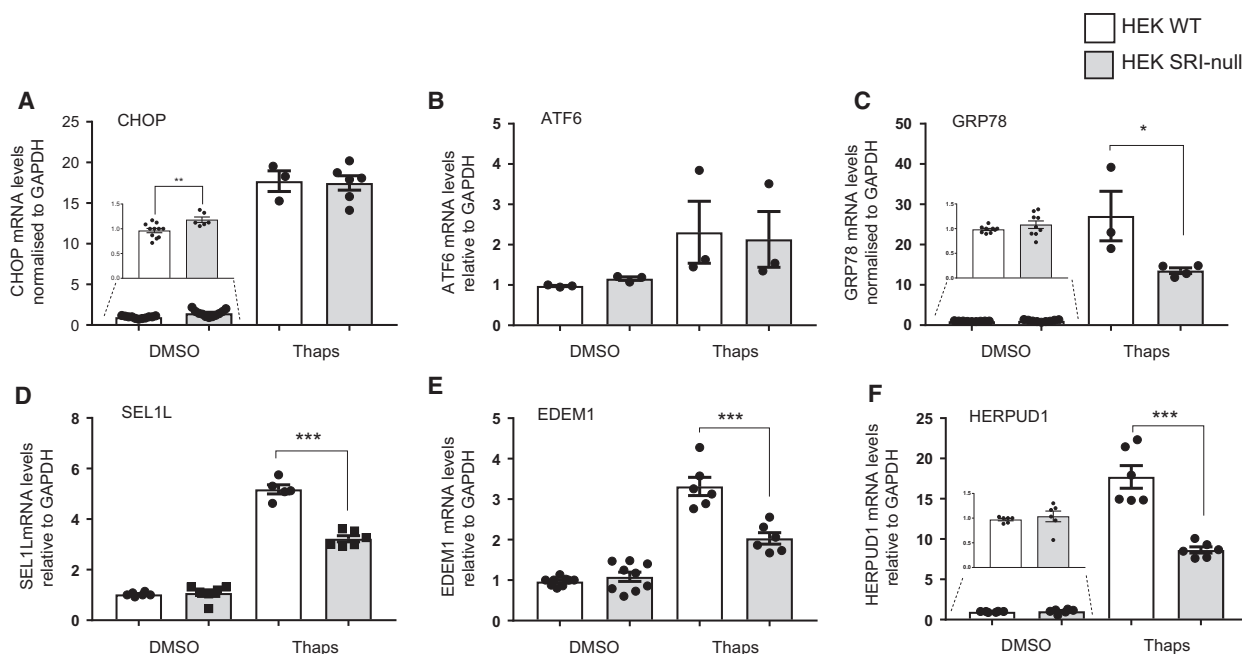


Fig. 4. Sorcin ablation impairs activation of ATF6 target genes during ER stress. (A–F) WT and *SRI*-null HEK293 cells were incubated with or without 0.1 μ M thapsigargin as indicated for 24 h before cell lysis and qRT-PCR analysis of CHOP (A), ATF6 (B) and four ATF6 target genes, namely GRP78 (C), SEL1L (D), EDEM1 (E) and HERPUD1 (F) as indicated. Results are expressed as means \pm SEM of ≥ 3 independent experiments, * $P < 0.05$ and *** $P < 0.001$ by two-tailed unpaired Student's *t*-tests.

affect the induction of CHOP and ATF6 itself by thapsigargin (Fig. 4A,B).

Sorcin increases ATF6 protein levels

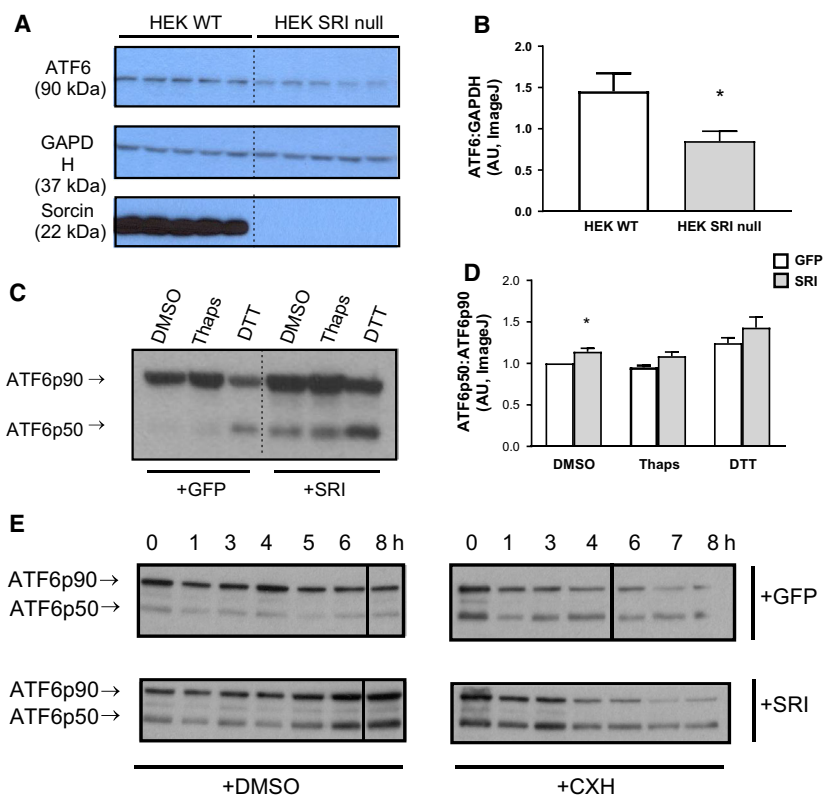
Intriguingly, despite slightly elevated or unchanged ATF6 mRNA levels in *SRI*-null vs WT HEK293 (Fig. 1F and 4B and not shown), endogenous ATF6 immunoreactivity was decreased in *SRI*-null HEK293 (Fig. 5A,B). This suggested a possible effect on ATF6 protein itself, either stability, activation or processing [30] rather than ATF6 transcription. Indeed, our data indicated that sorcin influenced both endogenous and exogenous ATF6 proteins, since we saw an effect on both p5xATF6-GL3 and p5xGAL4-Elb-GL3 reporters' activities following manipulation of sorcin protein levels.

To assess ATF6 processing, we cotransfected HEK293 cells with 3xFLAG-ATF6 together with either sorcin or GFP as control and treated the cells with thapsigargin or dithiothreitol (DTT) to measure the relative proportion of ATF6p50 (cleaved) to ATF6p90 (full length) by western blotting using an anti-FLAG antibody. As shown in Fig. 5C,D, a small (~14%) but reproducible and significant increases were found in the ratios of ATF6p50 band intensity to

ATF6p90 band intensity when ATF6 was co-expressed with sorcin compared to GFP in basal condition, although this became less significant in the presence of high dose thapsigargin (1 μ M) or DTT.

Since it has been reported that ATF6 cleavage is proportional to ATF6 abundance [42,46], we thus sought to investigate whether sorcin might prolong the half-life and/or the stability of ATF6 protein, which in turn would promote its processing and activation. ATF6 protein half-life is short, 2–3 h, [46,47] and ER stress increases ATF6 protein turnover by promoting its degradation through the proteasome [48–50]. It was therefore conceivable that, by reducing ER stress [22,51], sorcin might prolong the half-life and/or the stability of ATF6 protein. To test this hypothesis, HEK293 cells were cotransfected with 3xFLAG-ATF6 and sorcin or GFP for 24 h and incubated in the presence of cycloheximide (CXH) to stop de novo protein synthesis or DMSO (vehicle) for up to 8 h before immunoblotting. In control GFP/DMSO conditions (Fig. 5E, top left panel), total ATF6 protein abundance remained fairly constant over the 8-h period, whereas in the presence of overexpressed sorcin (Fig. 5E bottom left panel), there was an increase in the amount of both ATF6p90 and ATF6p50 band intensities. However,

Fig. 5. Sorcin increases ATF6 protein levels. (A) Representative western blot of endogenous ATF6, GAPDH and sorcin immunoreactivity in WT and *SRI*-null HEK293 cells and (B) quantification of ATF6:GAPDH ratios of 12 samples from 2 independent western blots by IMAGEJ as described in Methods. (C, D) HEK293 cells were transfected with 3xFLAG-ATF6 and either sorcin or GFP expression vectors as indicated for a total of 48 h. Thapsigargin 1 μ M and DTT 10 mM were added 16 h and 1 h, respectively, before cell lysis and western blotting using a monoclonal anti-Flag antibody. (C) shows a representative western blot, (D) shows a quantification of ATF6p50:ATF6p90 ratios of 3 independent western blots by ImageJ. * $P < 0.05$ by two-tailed unpaired Student's *t*-tests. (E) Representative western blots showing anti-Flag immunoreactivity in HEK293 cells transfected with 3xFLAG-ATF6 and either sorcin or GFP expression vectors as indicated for 24 h before the addition of 50 μ g/mL cycloheximide (CHX) or DMSO. Samples were collected for up to 8 h after treatment as indicated.



in the presence of CXH (Fig. 5E, right panels), there was a noticeable decline in ATF6p90 immunoreactivity after 3 h, compatible with the reported half-life of ATF6, and a near-complete disappearance after 7 h, which sorcin overexpression failed to alter compared with GFP.

We next sought to evidence a direct interaction between sorcin and ATF6 as this could provide some explanations about the mechanism(s) behind the stimulatory effect of sorcin on ATF6 signalling. Such interaction has been reported *in vitro* by Lalioti *et al.* using a protein array [52] and mentioned in an abstract published by Colotti *et al.* [53].

We therefore performed confocal microscopy colocalization studies, Förster/fluorescence resonance energy transfer (FRET) experiments using the acceptor-photobleaching FRET (ap-FRET) technique [54] and co-immunoprecipitation (Co-IP) experiments. A schematic representation of the different constructs used is shown in Fig. S2A.

As shown in Fig. 6A, confocal microscopy analysis of HEK cells cotransfected with sorcin tagged to mVenus (YFP-SRI) and the ER tracker DsRed2-ER-5 do not show a strong colocalization of sorcin in the ER, but rather a diffuse soluble pattern. A similar result was obtained with HA-tagged sorcin (not shown).

FRET efficiencies were measured between mVenus-tagged sorcin (YFP-SRI) and CFP-ATF6 (mCerulean tag on the N-terminal side of ATF6, intracytosolic) or ATF6-CFP (mCerulean tag on the C-terminal end of ATF6, intra-ER). Positive control was reference standard vector C5V, where mCerulean and mVenus are separated by five amino acids (35). Negative controls included the pairs CFP-ATF6/YFP alone, CFP alone/YFP-SRI and CFP/YFP.

As shown in Fig. 6B, in basal nontreated conditions, the FRET efficiency of the reference standard C5V was $24.90\% \pm 0.95\%$, whereas the FRET efficiency of the negative controls CFP-ATF6/YFP, CFP/YFP-SRI and CFP/YFP was $7.75\% \pm 1.09\%$, $5.30\% \pm 0.35\%$ and $5.63\% \pm 0.53\%$, respectively. In comparison, the FRET efficiency of CFP-ATF6/YFP-SRI was $9.03\% \pm 1.20\%$, and the pair ATF6-CFP and YFP-SRI gave a FRET efficiency of $11.43\% \pm 1.30\%$. Only the FRET signal for the pair ATF6-CFP (C-terminal fluorescent tag, intra-ER) and YFP-SRI was significantly higher than the negative control CFP+YFP-SRI. Individual traces of mCerulean fluorescence before and after photobleaching of mVenus are shown in Fig. S3, together with representative images showing HEK293 cells transfected with the different FRET constructs before and after photobleaching.

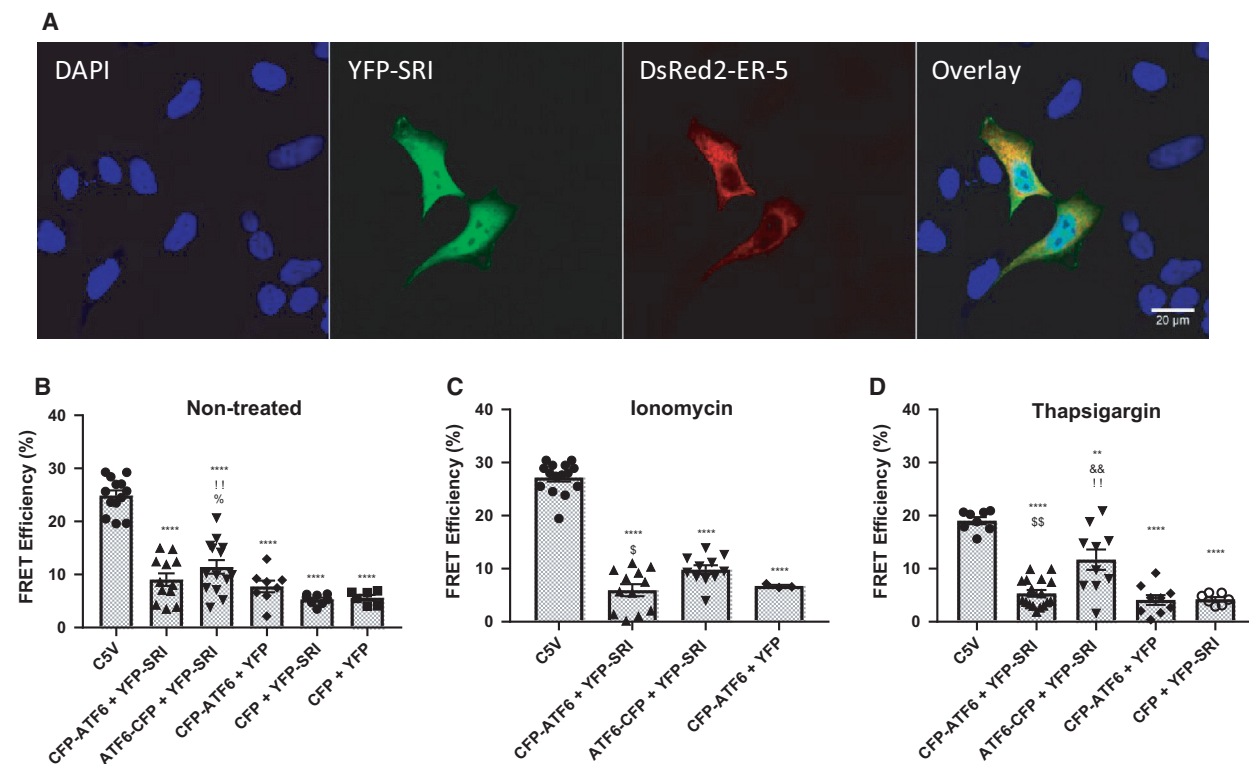


Fig. 6. Sorcin and ATF6 protein interaction studies (A) Representative images of wild-type HEK293T cells cotransfected with YFP-SRI and DsRed2-ER-5, an ER marker, and mounted with DAPI to determine nuclear localization. Images were acquired and analysed as described in Methods. (B–D) Quantification of the FRET efficiency between the pairs of proteins indicated below the graphs, in nontreated cells (B), in ionomycin-treated cells (1 μM for 1 h) (C) and in thapsigargin-treated cells (0.03 μM for 24 h) (D). Mean fluorescence intensity with excitation at 405 nm was calculated before and after photobleaching of regions of interest and FRET efficiency calculated as detailed in Methods. Significance was calculated using two-tailed Student's *t*-test for unpaired data, with Tukey's multiple comparison test and ANOVA. *n* is indicated by the individual points, *, **, **** indicate *P* < 0.05, 0.01 and 0.0001, respectively. Symbols represent the *P* values for the following *t*-tests: * vs C5V, ! vs CFP+YFP-SRI, % vs CFP+YFP, \$ vs ATF6-CFP+YFP-SRI, & vs CFP-ATF6.

In ionomycin-treated cells, which increased intracellular $[Ca^{++}]$ by 2.4-fold (not shown), the FRET efficiency of C5V was $27.17\% \pm 0.76\%$ and was $6.73\% \pm 0.21\%$ for the negative control CFP-ATF6 + YFP. FRET efficiency between ATF6-CFP and YFP-SRI was $9.83\% \pm 0.81\%$ and $5.95\% \pm 1.13\%$ for the CFP-ATF6 + YFP-SRI combination (Fig. 5B).

Finally, in thapsigargin-treated cells (Fig. 5C), the FRET efficiency was $19.04\% \pm 0.67\%$ for C5V and $4.11\% \pm 0.91\%$ and $4.26\% \pm 0.40\%$ for the negative controls CFP-ATF6/YFP and CFP/YFP-SRI, respectively. As in nontreated cells, the FRET efficiency between the C terminally tagged ATF6 protein ATF6-CFP and YFP-SRI ($11.71\% \pm 1.91\%$) was significantly higher than the negative control pairs and also higher than the FRET efficiency of CFP-ATF6/YFP-SRI ($5.35\% \pm 0.64\%$).

A higher FRET efficiency between sorcin and ATF6 when the fluorophore was on the C-terminal

end of ATF6, that is inside the ER, would imply sorcin presence inside the ER lumen in order to interact with ATF6. However, cellular fractionation experiments performed in HEK293 cells show that sorcin is located in the soluble cytosolic fraction, not inside the organelles such as GRP78 (Fig. S2C). The addition of fluorescent tags did not modify the sub-cellular location of either sorcin or ATF6 (not shown).

Also, despite the FRET experiments results above suggesting a possible interaction between the C-terminal end of ATF6 and sorcin, repeated attempts to Co-IP sorcin (endogenous or overexpressed) and either N-terminal (Flag or GFP/CFP tagged) or C-terminal CFP-tagged ATF6 constructs were unsuccessful. However, ATF6-CFP, with the CFP epitope located inside the ER, brought down GRP78, a known intra-ER-resident protein previously shown to interact with ATF6 inside the ER [55] (Fig. S2B).

Discussion

We have presented here a novel intracellular signalling pathway in the phenomena known as lipotoxicity [56], namely a decrease in sorcin expression induced by saturated fat, which in turn compromises ATF6 signalling and transcriptional activity. We show that palmitate decreases sorcin expression in HEK293 cells, used as a prototype for nonexcitable cells, where sorcin's roles have been less examined. The precise signalling pathway responsible for this effect of palmitate on sorcin expression is still unidentified, but could likely include palmitoylation, TNF α , NF κ B or Toll-like receptor 4 signalling [57].

ATF6 is one of the three ER-resident transmembrane protein sensors that are activated during the UPR, with PKR-like ER kinase (PERK) and inositol-requiring protein-1 (IRE1). Perturbations in ER homeostasis (accumulation of unfolded proteins, decreased ER Ca²⁺ content, etc.) activate the three branches in parallel to restore ER function. If the UPR is unsuccessful, the cell will undergo apoptosis [58]. Accumulation of misfolded proteins in the ER results in the dissociation of BiP/GRP78 from the C terminus of ATF6, unmasking a Golgi localization domain. In the Golgi, ATF6 is processed to its active form through sequential cleavage by site-1 and site-2 proteases (S1P and S2P) [59]. The N-terminal cytosolic portion of ATF6 containing a basic leucine zipper motif then translocates to the nucleus and acts as a transcription factor to stimulate the transcription of ER chaperones in order to restore ER homeostasis [46].

ATF6 activation is considered to be the prosurvival branch of the UPR, improving stroke outcomes [60] and myocardial ischaemia/reperfusion injury [61,62]. In the pancreatic beta cell, ATF6 is needed for beta-cell proliferation and compensation during insulin resistance [25] and ATF6-null mice do not display any defects in β -cell function on a normal chow diet but experience severe ER stress with reduced insulin content during HFD [24]. In the liver, ATF6 promotes fatty acid oxidation and attenuates hepatic steatosis in mice [63]. These results indicate that ATF6 has an important role in mitigating lipotoxicity during the progression of obesity and insulin resistance.

Here, we have shown that sorcin was necessary for optimum ATF6 transcriptional activity. Indeed, stimulation of ATF6 target genes during ER stress was reduced in the absence of sorcin (Fig. 4). Using two different *firefly* luciferase reporters, namely p5xATF6-GL3 and p5xGAL4-E1b-GL3, we showed that endogenous and exogenous ATF6 trans-activation ability was stimulated or inhibited following sorcin

overexpression or deletion, respectively (Fig. 2). The naturally occurring sorcin mutant F112L was as effective as WT sorcin in activating the UPRE reporter p5xATF6-GL3, despite an apparent increase in ER calcium, consistent with findings previously described in cardiac myocytes [44]. The combination of p5xGAL4-E1b-GL3 and pHA-GAL4-ATF6 was used to exclude an effect of sorcin on XBP1s, reported to bind the UPRE of p5xATF6-GL3 [42].

Our experiments point towards several possible mechanistical explanations for sorcin's potentiation of ATF6 activity, but more work will be needed to provide a definitive answer. Firstly, the activation seems to be independent of ER stress. Indeed, the pGLuc/ATF6LD-CLuc construct, encoding only the C-terminal luminal domain of ATF6 fused to a secreted luciferase, is less secreted in the absence of sorcin, despite ER stress being observed (Fig. 1F and 3B). Secondly, the positive effect of sorcin on ATF6 abundance and processing is not transcriptional (Fig. 1F) but we could not evidence an increase in ATF6 stability (Fig. 5) or confirm a direct interaction between the two proteins by Co-IP or confocal microscopy (Fig. 6). Our ap-FRET experiments pointed towards a possible interaction inside the ER (Fig. 6B), but despite others showing sorcin to be present in the cytoplasm and the ER of 3T3-L1 fibroblasts by cellular fractionation [52], we could not evidence this in HEK cells (Fig. S2C). FRET transfer occurs over a range between 1 and 10 nm, and the thickness of the bilayers of the ER membrane is approximately 3.75 nm [64] leaving some possibility that sorcin and ATF6 are not directly interacting with each other but that the FRET signal observed could in fact be occurring across the ER membrane. It is, however, possible that the interaction is highly localized in cell microenvironment, possibly at MAMs [53], or through a dynamic protein complex, possibly involving WFS1 (Fig. 1F) [50] and was missed in our experimental conditions.

In conclusion, our experiments have shown that sorcin is necessary for full ATF6 activation and transcriptional activity during ER stress and that lipotoxicity impairs sorcin expression, potentially contributing to defects observed in a wide range of tissues during the progression of obesity.

Acknowledgements

Funding was provided by Imperial College London and grants to IL from Diabetes UK (BDA:12/0004535 and BDA:16/0005485) and The Rosetrees Trust (A1063); to GAR from the Wellcome Trust (WT098424AIA and 212625/Z/18/Z), the MRC (MR/R022259/1,

MR/J0003042/1, MR/L020149/1 and MR/N00275X/1) and Diabetes UK (BDA/15/0005275). The authors thank Prof Ron Prywes (Columbia University) and Prof Gökhan Hotamisligil (Harvard University) for providing plasmids and Stephen Rothery of the FILM facility at Imperial College London (<http://www.imperial.ac.uk/medicine/facility-for-imaging-by-light-microscopy/>) for help with FRET imaging studies.

Conflict of interest

GAR has received grant support from Sun Pharma and from Servier.

Author contributions

SP, TG, NJA, JA and IL performed experiments and analysed data. IL, PLC, SP and GAR designed experiments. DVK, HHV, GAR and IL contributed resources. IL and SP wrote the manuscript. IL is the guarantor of this work and takes responsibility for the integrity and accuracy of the data presented.

Data accessibility

The data that support the findings of this study are available from the corresponding author [i.leclerc@imperial.ac.uk] upon reasonable request.

References

- Whitlock G, Lewington S, Sherliker P, Clarke R, Emberson J, Halsey J, Qizilbash N, Collins R and Peto R (2009) Body-mass index and cause-specific mortality in 900 000 adults: collaborative analyses of 57 prospective studies. *Lancet* **373**, 1083–1096.
- Oyadomari S, Koizumi A, Takeda K, Gotoh T, Akira S, Araki E and Mori M (2002) Targeted disruption of the Chop gene delays endoplasmic reticulum stress-mediated diabetes. *J Clin Invest* **109**, 525–532.
- Cunha DA, Hekerman P, Ladriere L, Bazarra-Castro A, Ortis F, Wakeham MC, Moore F, Rasschaert J, Cardozo AK, Bellomo E *et al.* (2008) Initiation and execution of lipotoxic ER stress in pancreatic beta-cells. *J Cell Sci* **121**, 2308–2318.
- Ozcan U, Cao Q, Yilmaz E, Lee AH, Iwakoshi NN, Ozdelen E, Tuncman G, Gorgun C, Glimcher LH and Hotamisligil GS (2004) Endoplasmic reticulum stress links obesity, insulin action, and type 2 diabetes. *Science* **306**, 457–461.
- Boden G, Duan X, Homko C, Molina EJ, Song W, Perez O, Cheung P and Merali S (2008) Increase in endoplasmic reticulum stress-related proteins and genes in adipose tissue of obese, insulin-resistant individuals. *Diabetes* **57**, 2438–2444.
- Koh HJ, Toyoda T, Didesch MM, Lee MY, Sleeman MW, Kulkarni RN, Musi N, Hirshman MF and Goodyear LJ (2013) Tribbles 3 mediates endoplasmic reticulum stress-induced insulin resistance in skeletal muscle. *Nat Commun* **4**, 1871.
- Ozcan L, Ergin AS, Lu A, Chung J, Sarkar S, Nie D, Myers MG Jr and Ozcan U (2009) Endoplasmic reticulum stress plays a central role in development of leptin resistance. *Cell Metab* **9**, 35–51.
- Guerrero-Hernandez A, Leon-Aparicio D, Chavez-Reyes J, Olivares-Reyes JA and DeJesus S (2014) Endoplasmic reticulum stress in insulin resistance and diabetes. *Cell Calcium* **56**, 311–322.
- Colotti G, Poser E, Fiorillo A, Genovese I, Chiarini V and Ilari A (2014) Sorcin, a calcium binding protein involved in the multidrug resistance mechanisms in cancer cells. *Molecules* **19**, 13976–13989.
- Valdivia HH (1998) Modulation of intracellular Ca²⁺ levels in the heart by sorcin and FKBP12, two accessory proteins of ryanodine receptors. *Trends Pharmacol Sci* **19**, 479–482.
- Ilari A, Johnson KA, Nastopoulos V, Verzili D, Zamparelli C, Colotti G, Tsernoglou D and Chiancone E (2002) The crystal structure of the sorcin calcium binding domain provides a model of Ca²⁺-dependent processes in the full-length protein. *J Mol Biol* **317**, 447–458.
- Van der Blik AM, Meyers MB, Biedler JL, Hes E and Borst P (1986) A 22-kd protein (sorcin/V19) encoded by an amplified gene in multidrug-resistant cells, is homologous to the calcium-binding light chain of calpain. *Embo J* **5**, 3201–3208.
- Maki M, Kitaura Y, Satoh H, Ohkouchi S and Shibata H (2002) Structures, functions and molecular evolution of the penta-EF-hand Ca²⁺-binding proteins. *Biochim Biophys Acta* **1600**, 51–60.
- Appelblom H, Nurmi J, Soukka T, Pasternack M, Penttila KE, Lovgren T and Niemela P (2007) Homogeneous TR-FRET high-throughput screening assay for calcium-dependent multimerization of sorcin. *J Biomol Screen* **12**, 842–848.
- Chen X, Weber C, Farrell ET, Alvarado FJ, Zhao YT, Gomez AM and Valdivia HH (2017) Sorcin ablation plus beta-adrenergic stimulation generate an arrhythmogenic substrate in mouse ventricular myocytes. *J Mol Cell Cardiol* **114**, 199–210.
- Meyers MB and Biedler JL (1981) Increased synthesis of a low molecular weight protein in vincristine-resistant cells. *Biochem Biophys Res Commun* **99**, 228–235.
- Lokuta AJ, Meyers MB, Sander PR, Fishman GI and Valdivia HH (1997) Modulation of cardiac ryanodine receptors by sorcin. *J Biol Chem* **272**, 25333–25338.

- 18 Fabiato A (1983) Calcium-induced release of calcium from the cardiac sarcoplasmic reticulum. *Am J Physiol* **245**, C1–14.
- 19 Farrell EF, Antaramian A, Rueda A, Gomez AM and Valdivia HH (2003) Sorcin inhibits calcium release and modulates excitation-contraction coupling in the heart. *J Biol Chem* **278**, 34660–34666.
- 20 Stern MD and Cheng H (2004) Putting out the fire: what terminates calcium-induced calcium release in cardiac muscle? *Cell Calcium* **35**, 591–601.
- 21 Matsumoto T, Hisamatsu Y, Ohkusa T, Inoue N, Sato T, Suzuki S, Ikeda Y and Matsuzaki M (2005) Sorcin interacts with sarcoplasmic reticulum Ca(2+)-ATPase and modulates excitation-contraction coupling in the heart. *Basic Res Cardiol* **100**, 250–262.
- 22 Marmugi A, Parnis J, Chen X, Carmichael L, Hardy J, Mannan N, Marchetti P, Piemonti L, Bosco D, Johnson P *et al.* (2016) Sorcin links pancreatic beta cell lipotoxicity to ER Ca²⁺ stores. *Diabetes* **64**, 1009–1021.
- 23 Wang Y, Vera L, Fischer WH and Montminy M (2009) The CREB coactivator CRTC2 links hepatic ER stress and fasting gluconeogenesis. *Nature* **460**, 534–537.
- 24 Usui M, Yamaguchi S, Tanji Y, Tominaga R, Ishigaki Y, Fukumoto M, Katagiri H, Mori K, Oka Y and Ishihara H (2012) Atf6alpha-null mice are glucose intolerant due to pancreatic beta-cell failure on a high-fat diet but partially resistant to diet-induced insulin resistance. *Metabolism* **61**, 1118–1128.
- 25 Sharma RB, O'Donnell AC, Stamateris RE, Ha B, McCloskey KM, Reynolds PR, Arvan P and Alonso LC (2015) Insulin demand regulates beta cell number via the unfolded protein response. *J Clin Invest* **125**, 3831–3846.
- 26 Arruda AP and Hotamisligil GS (2015) Calcium homeostasis and organelle function in the pathogenesis of obesity and diabetes. *Cell Metab* **22**, 381–397.
- 27 Ozcan U, Yilmaz E, Ozcan L, Furuhashi M, Vaillancourt E, Smith RO, Gorgun CZ and Hotamisligil GS (2006) Chemical chaperones reduce ER stress and restore glucose homeostasis in a mouse model of type 2 diabetes. *Science* **313**, 1137–1140.
- 28 Noordeen NA, Meur G, Rutter GA and Leclerc I (2012) Glucose-induced nuclear shuttling of ChREBP is mediated by sorcin and Ca(2+) ions in pancreatic beta-cells. *Diabetes* **61**, 574–585.
- 29 Wang Y, Shen J, Arenzana N, Tirasophon W, Kaufman RJ and Prywes R (2000) Activation of ATF6 and an ATF6 DNA binding site by the endoplasmic reticulum stress response. *J Biol Chem* **275**, 27013–27020.
- 30 Chen X, Shen J and Prywes R (2002) The luminal domain of ATF6 senses endoplasmic reticulum (ER) stress and causes translocation of ATF6 from the ER to the Golgi. *J Biol Chem* **277**, 13045–13052.
- 31 Fu S, Yalcin A, Lee GY, Li P, Fan J, Arruda AP, Pers BM, Yilmaz M, Eguchi K and Hotamisligil GS (2015) Phenotypic assays identify azoramide as a small-molecule modulator of the unfolded protein response with antidiabetic activity. *Sci Transl Med* **7**, 292ra98.
- 32 Kracht MJL, de Koning EJP, Hoeben RC, Roep BO and Zaldumbide A (2018) Bioluminescent reporter assay for monitoring ER stress in human beta cells. *Sci Rep* **8**, 17738.
- 33 Gade P, Ramachandran G, Maachani UB, Rizzo MA, Okada T, Prywes R, Cross AS, Mori K and Kalvakolanu DV (2012) An IFN-gamma-stimulated ATF6-C/EBP-beta-signaling pathway critical for the expression of Death Associated Protein Kinase 1 and induction of autophagy. *Proc Natl Acad Sci USA* **109**, 10316–10321.
- 34 Koushik SV, Chen H, Thaler C, Puhl HL and Vogel SS (2006) Cerulean, Venus, and Venus(Y67C) FRET reference standards. *Biophys J* **91**, L99–L101.
- 35 Day RN and Davidson MW (2009) The fluorescent protein palette: tools for cellular imaging. *Chem Soc Rev* **38**, 2887–2921.
- 36 Chen X, Weber C, Farrell ET, Alvarado FJ, Zhao YT, Gomez AM and Valdivia HH (2018) Sorcin ablation plus beta-adrenergic stimulation generate an arrhythmogenic substrate in mouse ventricular myocytes. *J Mol Cell Cardiol* **114**, 199–210.
- 37 Jozefczuk J, Drews K and Adjaye J (2012) Preparation of mouse embryonic fibroblast cells suitable for culturing human embryonic and induced pluripotent stem cells. *J Vis Exp* **64**, 3854.
- 38 Ran FA, Hsu PD, Wright J, Agarwala V, Scott DA and Zhang F (2013) Genome engineering using the CRISPR-Cas9 system. *Nat Protoc* **8**, 2281–2308.
- 39 Sun G, Tarasov AI, McGinty JA, French PM, McDonald A, Leclerc I and Rutter GA (2010) LKB1 deletion with the RIP2.Cre transgene modifies pancreatic beta-cell morphology and enhances insulin secretion in vivo. *Am J Physiol Endocrinol Metab* **298**, E1261–E1273.
- 40 Ravier MA and Rutter GA (2010) Isolation and culture of mouse pancreatic islets for ex vivo imaging studies with trappable or recombinant fluorescent probes. *Methods Mol Biol* **633**, 171–184.
- 41 Holden P and Horton WA (2009) Crude subcellular fractionation of cultured mammalian cell lines. *BMC Res Notes* **2**, 243.
- 42 Shen J and Prywes R (2005) ER stress signaling by regulated proteolysis of ATF6. *Methods* **35**, 382–389.
- 43 Franceschini S, Ilari A, Verzili D, Zamparelli C, Antaramian A, Rueda A, Valdivia HH, Chiancone E and Colotti G (2008) Molecular basis for the impaired function of the natural F112L sorcin mutant: X-ray crystal structure, calcium affinity, and interaction with annexin VII and the ryanodine receptor. *FASEB J* **22**, 295–306.
- 44 Collis LP, Meyers MB, Zhang J, Phoon CK, Sobie EA, Coetzee WA and Fishman GI (2007) Expression of a

- sorcin missense mutation in the heart modulates excitation-contraction coupling. *FASEB J* **21**, 475–487.
- 45 Fu S, Yang L, Li P, Hofmann O, Dicker L, Hide W, Lin X, Watkins SM, Ivanov AR and Hotamisligil GS (2011) Aberrant lipid metabolism disrupts calcium homeostasis causing liver endoplasmic reticulum stress in obesity. *Nature* **473**, 528–531.
- 46 Haze K, Yoshida H, Yanagi H, Yura T and Mori K (1999) Mammalian transcription factor ATF6 is synthesized as a transmembrane protein and activated by proteolysis in response to endoplasmic reticulum stress. *Mol Biol Cell* **10**, 3787–3799.
- 47 Teske BF, Wek SA, Bunpo P, Cundiff JK, McClintick JN, Anthony TG and Wek RC (2011) The eIF2 kinase PERK and the integrated stress response facilitate activation of ATF6 during endoplasmic reticulum stress. *Mol Biol Cell* **22**, 4390–4405.
- 48 Hong M, Li M, Mao C and Lee AS (2004) Endoplasmic reticulum stress triggers an acute proteasome-dependent degradation of ATF6. *J Cell Biochem* **92**, 723–732.
- 49 Yoshida H, Uemura A and Mori K (2009) pXBP1(U), a negative regulator of the unfolded protein response activator pXBP1(S), targets ATF6 but not ATF4 in proteasome-mediated degradation. *Cell Struct Funct* **34**, 1–10.
- 50 Fonseca SG, Ishigaki S, Osowski CM, Lu S, Lipson KL, Ghosh R, Hayashi E, Ishihara H, Oka Y, Permutt MA *et al.* (2010) Wolfram syndrome 1 gene negatively regulates ER stress signaling in rodent and human cells. *J Clin Invest* **120**, 744–755.
- 51 Maddalena F, Laudiero G, Piscazzi A, Secondo A, Scorziello A, Lombardi V, Matassa DS, Fersini A, Neri V, Esposito F *et al.* (2011) Sorcin induces a drug-resistant phenotype in human colorectal cancer by modulating Ca²⁺ homeostasis. *Cancer Res* **71**, 7659–7669.
- 52 Lalioti VS, Ilari A, O'Connell DJ, Poser E, Sandoval IV and Colotti G (2014) Sorcin links calcium signaling to vesicle trafficking, regulates Polo-like kinase 1 and is necessary for mitosis. *PLoS ONE* **9**, e85438.
- 53 Colotti G, Genovese I, Bidollari E, Rosati J, Perluigi M, Cali T, Arena A, Squitieri F and Ilari A (2018) Sorcin Rescues Ca (Ii) Dysregulation and Endoplasmic Reticulum Stress in Huntington's Disease. *J Neurol Neurosurg Ps* **89**, A8.
- 54 Snapp EL and Hegde RS (2006) Rational design and evaluation of FRET experiments to measure protein proximities in cells. *Curr Protoc Cell Biol* **17**, 9.
- 55 Shen J, Chen X, Hendershot L and Prywes R (2002) ER stress regulation of ATF6 localization by dissociation of BiP/GRP78 binding and unmasking of Golgi localization signals. *Dev Cell* **3**, 99–111.
- 56 Poirout V and Robertson RP (2008) Glucolipototoxicity: fuel excess and beta-cell dysfunction. *Endocr Rev* **29**, 351–366.
- 57 Fatima S, Hu X, Gong RH, Huang C, Chen M, Wong HLX, Bian Z and Kwan HY (2019) Palmitic acid is an intracellular signaling molecule involved in disease development. *Cell Mol Life Sci* **76**, 2547–2557.
- 58 Szegezdi E, Logue SE, Gorman AM and Samali A (2006) Mediators of endoplasmic reticulum stress-induced apoptosis. *EMBO Rep* **7**, 880–885.
- 59 Ye J, Rawson RB, Komuro R, Chen X, Dave UP, Prywes R, Brown MS and Goldstein JL (2000) ER stress induces cleavage of membrane-bound ATF6 by the same proteases that process SREBPs. *Mol Cell* **6**, 1355–1364.
- 60 Yu Z, Sheng H, Liu S, Zhao S, Glembotski CC, Warner DS, Paschen W and Yang W (2017) Activation of the ATF6 branch of the unfolded protein response in neurons improves stroke outcome. *J Cereb Blood Flow Metab* **37**, 1069–1079.
- 61 Jin JK, Blackwood EA, Azizi K, Thuerauf DJ, Fahem AG, Hofmann C, Kaufman RJ, Doroudgar S and Glembotski CC (2017) ATF6 decreases myocardial ischemia/reperfusion damage and links ER stress and oxidative stress signaling pathways in the heart. *Circ Res* **120**, 862–875.
- 62 Blackwood EA, Azizi K, Thuerauf DJ, Paxman RJ, Plate L, Kelly JW, Wiseman RL and Glembotski CC (2019) Pharmacologic ATF6 activation confers global protection in widespread disease models by reprogramming cellular proteostasis. *Nat Commun* **10**, 187.
- 63 Chen X, Zhang F, Gong Q, Cui A, Zhuo S, Hu Z, Han Y, Gao J, Sun Y, Liu Z *et al.* (2016) Hepatic ATF6 increases fatty acid oxidation to attenuate hepatic steatosis in mice through peroxisome proliferator-activated receptor alpha. *Diabetes* **65**, 1904–1915.
- 64 Mitra K, Ubarretxena-Belandia I, Taguchi T, Warren G and Engelman DM (2004) Modulation of the bilayer thickness of exocytic pathway membranes by membrane proteins rather than cholesterol. *Proc Natl Acad Sci USA* **101**, 4083–4088.

Supporting information

Additional supporting information may be found online in the Supporting Information section at the end of the article.

Fig. S1. (A) Responsiveness of p5xATF6 luciferase reporter to ATF6. (B) Lack of effect of sorcin ablation on four unrelated luciferase reporters.

Fig. S2. (A) Schematic representation of the constructs used in co-IP and apFRET experiments. (B) Representative co-IP experiment.

Fig. S3. (A–D) mCerulean fluorescence traces of HEK293 cells transfected with the indicated constructs before and after mVenus photobleaching.